Evidence of Surface-Preferential Co Distribution in ZnO Nanocrystal and Its Effects on the Ferromagnetic Property

Weichang Hao,*,† Jianjun Li,† Huaizhe Xu,‡ Jiaou Wang,§ and Tianmin Wang†

Center of Materials Physics and Chemistry and Department of Physics, Beihang University, Beijing 100191, P. R. China, and Beijing Synchrotron Radiation Facility, Institute of High Energy Physics, Chinese Academy of Sciences, 100049, P. R. China

ABSTRACT $Zn_{0.95}Co_{0.05}O$ nanocrystals were synthesized by the sol−gel method. A STEM image clearly shows that the Co in ZnO nanocrystals is of surface-preferential. To further study the distribution state of Co element and its effects on the structure and magnetic property, were postannealed the $Zn_{0.95}Co_{0.05}O$ nanocrystals in O_2, Ar, and H_2 atmospheres. It is found that the ferromagnetisms of the H_2- and Ar-annealed $Zn_{0.95}Co_{0.05}O$ nanocrystals increase significantly, but that of the O_2-annealed sample decreases. The ferromagnetism variations of the Ar- and O_2-annealed sample are stemmed from the increase of oxygen vacancies (V_o) and the formation of second-phase Co_3O_4, respectively, whereas the great enhancement of ferromagnetism in the H_2-annealed sample is attributed to the appearance of interstitial H (H_i) related defects. Our results indicate that inhomogeneous Co distribution is helpful for manipulating the states of the Co ions and the ferromagnetic coupling in $Zn_{1-x}Co_xO$ by post-treatment.

KEYWORDS: surface-preferential distribution • ZnO • ferromagnetic property • postannealing

1. INTRODUCTION

Diluted magnetic semiconductors (DMSs) have attracted extensive attentions due to their potential applications in spintronics (1). Theoretical calculations predict that transition-metal-doped ZnO is one of the most promising DMSs for realizing room-temperature ferromagnetism, which is a prerequisite for practical applications (2, 3). Tremendous efforts have been focused on ZnO-based DMSs (ZDMSs), especially on $Zn_{1-x}Co_xO$ and $Zn_{1-x}Mn_xO$. However, scattered results are frequently obtained by different groups using different experimental or characterization methods (4−7). The origin of the observed ferromagnetism is still under intense debate. Some groups believe that the ferromagnetism results from the random substitution of Zn by transition metal (TM) ions. But the mechanism of the magnetic coupling is hard to understand for the relatively long distance between TM ions (8). Other groups suggest that the ferromagnetism comes from the inhomogeneous distribution of TM element (e.g., rich Co distribution at the surface) or the presence of second-phase structures, such as TM metal or other TM compound clusters (9−11). Recent theoretical calculations also predict that the doped Co ions in $Zn_{1-x}Co_xO$ have the tendency to congregate, and it is easy to form second-phase clusters when the doping ratio further increases (12, 13). At the congregation area, the average distance between Co ions is shortened and the magnetic coupling between Co ions becomes stronger. Meanwhile, the defect structures in $Zn_{1-x}Co_xO$, which play important roles in mediating magnetic coupling, are also reported (14, 15). Thus the inhomogeneous Co distribution has important effects on the magnetism of $Zn_{1-x}Co_xO$. Many experimental results reveal that the ferromagnetism variation with Co-doping concentration has a turning point, which is normally reported as 5% or 10% (16−18). The ferromagnetism increases with Co-doping until the turning point, and then decreases sharply beyond the point. The tuning point is often near the solid solubility, so the inhomogeneous Co distribution becomes more obvious at this doping concentration. In our sol−gel synthesized $Zn_{1-x}Co_xO$ nanocrystal samples, this turning point is repetitively obtained as 5%. With further increase of Co-doping, second-phase Co_3O_4 forms and the ferromagnetism declines quickly (19). To clearly determine whether there is obvious Co inhomogeneous distribution in $Zn_{1-x}Co_xO$ and its effect on the structure and ferromagnetism, and further understand the magnetic coupling mechanism in ZDMSs, we postannealed the $Zn_{0.95}Co_{0.05}O$ nanocrystals in argon, oxygen, and hydrogen atmospheres, respectively, and systemically investigated their structure and magnetism. Our results indicate that the distribution of Co element in $Zn_{0.95}Co_{0.05}O$ is of surface-preferential because of the self-purification mechanism in nanocrystal growth process. This inhomogeneous distribution is advantage to modulate the state of Co ions and the ferromagnetic coupling in $Zn_{1-x}Co_xO$ via postannealing. It is also found that not only oxygen vacancies (V_o) but also interstitial H (H_i) related defects can mediate the ferromagnetic coupling between Co ions. The latter can lead to even

* Corresponding author. E-mail: whao@buaa.edu.cn.
Received for review April 9, 2010 and accepted June 7, 2010
† Center of Materials Physics and Chemistry, Beihang University.
‡ Department of Physics, Beihang University.
§ Chinese Academy of Sciences.
DOI: 10.1021/am100303n

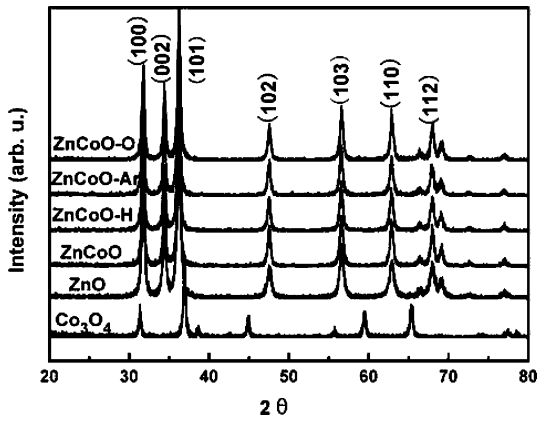

FIGURE 1. XRD spectra of ZnCoO, ZnCoO-O, ZnCoO-Ar, ZnCoO-H, ZnO, and Co_3O_4.

stronger ferromagnetism by forming Co−H−Co bridge bond structures.

2. EXPERIMENTAL SECTION

$Zn_{0.95}Co_{0.05}O$ nanocrystals were synthesized by the sol−gel method using $Zn(OAc)_2 \cdot 2H_2O$ and $Co(OAc)_2 \cdot 4H_2O$ as precursors and dimethyl sulfoxide as solvent. The detailed preparation process had been described previously (19, 20). After heating at 673 K for 2 h in air to burn up the organic component, the obtained powders were then respectively postannealed under O_2, Ar, and H_2/Ar (H_2, 60%; Ar, 40%) atmospheres at 673 K for 1 h. These four samples are named as ZnCoO, ZnCoO-O, ZnCoO-Ar, and ZnCoO-H, respectively.

The morphology and structures were investigated by transmission electronic microscopy (TEM, JEM-2100F), and X-ray diffraction (XRD, Rigaku D/Max-2200 XRD with Cu Kα source). The chemical state of Co and the detailed structure variations were characterized by XPS (MK II XPS with Al (Kα) source), X-ray near-edgy absorption spectroscopy (XNEAS) (using synchrotron radiation at Beijing Synchrotron Radiation Facility), and Raman (JY-T64000 micro-Raman spectrometer in the backscattering geometry excited by Ar^+ laser 532 nm line). The ferromagnetisms of the samples were measured by vibrating sample magnetometer (VSM, Lakeshore 7410) at room temperature in air.

3. RESULTS AND DISCUSSION

3.1. XRD and STEM Studies. Figure 1 shows the XRD spectra of ZnCoO, ZnCoO-O, ZnCoO-Ar, ZnCoO-H, pure ZnO nanocrystals, and commercial Co_3O_4. It is seen that all the annealed $Zn_{0.95}Co_{0.05}O$ nanocrystals have the similar wurtzite structure as pure ZnO (JCPDS data file 80-0074). No XRD peaks related to Co metal or Co_3O_4 can be observed. No second phase is detectable from the HRTEM image or from the corresponding Fast Fourier Transform (FFT) image, as shown Figure 2a. The crystal lattice in the HRTEM is measured as 0.247 nm, which is accordant with the (101) interplanar distance of wurtzite ZnO. From the TEM image of nanocrystals, it is found that the as-prepared $Zn_{1-x}Co_xO$ sample is sphere particle and about 17−23 nm in diameters. The size distribution of nanoparticle is about 20 ± 3 nm. Only Zn, Co, and O peaks are detectable in the energy dispersive spectrum shown in Figure 2b. The Zn to Co atomic ratio is measured as 95.2:4.8, very close to the nominal doping ratio of 95:5. Figure 2c shows the element distribution of Zn, Co, and O along the white line detected by scanning transmission electronic microscopy (STEM) line scanning mode. It is found that the O element distribution is uniform, whereas the distributions of Co and Zn element are inhomogeneous. The Co concentration at the surface area of the nanocrystal is obviously higher than that at the core area, which indicates that the Co distribution in $Zn_{0.95}Co_{0.05}O$ is of surface-preferential. As shown in STEM image, the thickness of the Co-rich surface layer is about 2−3 nm.

3.2. Formation Mechanism of Surface-Preferential Co Distribution. The sketches of detailed self-purification process are shown in Figure 3. In the dimethyl sulfoxide solution of Zn^{2+} and Co^{2+}, pure ZnO crystal nucleus form first when alkaline solution is added dropwise, whereas Co^{2+} ions is in an octahedral ligand environment (20, 21). Therefore, they are not ready for being doped into the ZnO lattice, where the doped Co^{2+} ions should mainly occupy the tetrahedral ligand field. With the increasing OH^- concentration, the ZnO crystal nucleus enlarge and the octahedral ligand field of Co^{2+} ions are introduced to tetrahedral field by the hydrolysis and condensation reaction of precursors. The DMSO solution changes from pink to blue with addition of OH^-, which indicates this conversion of octahedral Co^{2+} to tetrahedral Co^{2+} (21). Semiconductor nanocrystals doped with transition metals has proved to be particularly difficult (22−24). F. V. Mikulec and G. M. Dalpian attribute this phenomenon to self-purification mechanism (22, 23). This implies that the impurities are expelled on the surface of nanocrystals for thermodynamic reasons. We believe that this mechanism is also effective on our system, most of Co^{2+} dopants are expelled out of core area of nanocrystals, only a little part of the "doped" Co^{2+} ions are incorporated into the nanocrystal. As a result, the dopant concentration increases in grads from the core to the shell.

Because Co distribution in the nanocrystals is of surface-preferential, Co concentration at the surface area is very large, thus the average distance between Co ions is small. This should have great effects on the structure and properties of the $Zn_{1-x}Co_xO$ nanocrystals. First, the ferromagnetic coupling between Co ions becomes more easily for the small Co distance at the surface area. In fact, some of the recent works shown that the ferromagnetism of $Zn_{1-x}Co_xO$ mainly originates from the surface or interface (14, 15). Second, the density of Co ions at the surface area is very high, it can even approach the bulk solubility, and thus the substitutional Co ions are nearly saturated. In this case, some of the Co ions can occupy the interstitial sites for system energy optimization. Because the interstitial Co ions are of substable state, their chemical state and properties should be easily controlled by the outer treatments, including postannealing, codoping, and surface treatment. Our postannealing experiment clearly proves this deduction.

3.3. *M*−*H* Curves. Figure 4 shows the room-temperature *M*−*H* curves of all the samples. The measured ferromagnetisms of ZnCoO, ZnCoO-O, ZnCoO-Ar, and ZnCoO-H are 0.0021, 0.0018, 0.0040, and 0.022 emu/g, respectively. After O_2 annealing, the magnetism of the $Zn_{0.95}Co_{0.05}O$

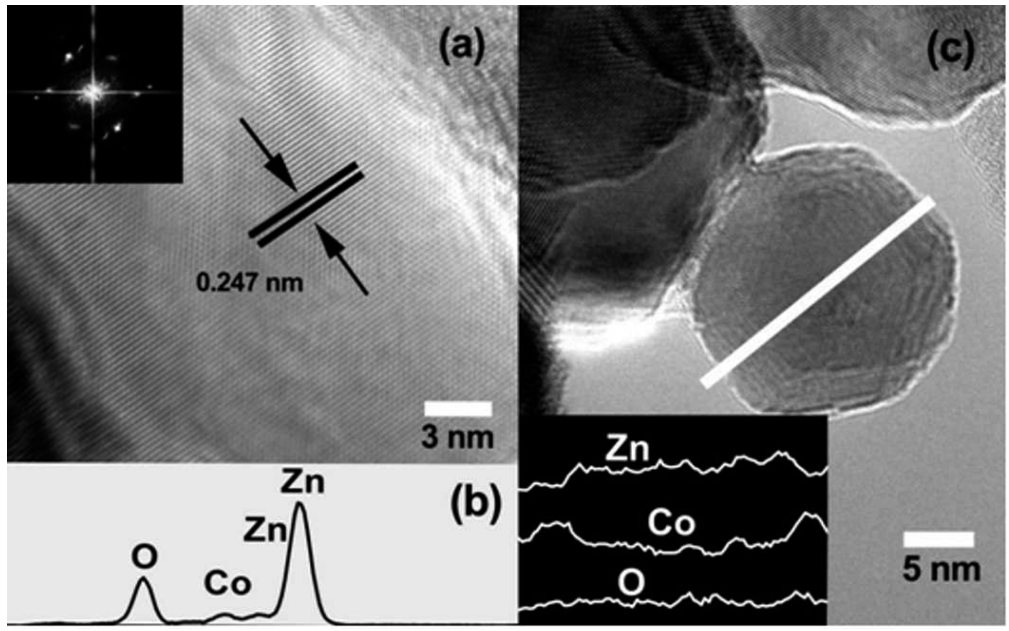

FIGURE 2. (a) HRTEM image (inset, the correspondent FFT pattern), (b) EDS spectrum of ZnCoO-H, and (c) TEM image (inset, the element distribution of Co, Zn, and O, detected by STEM) of ZnCoO.

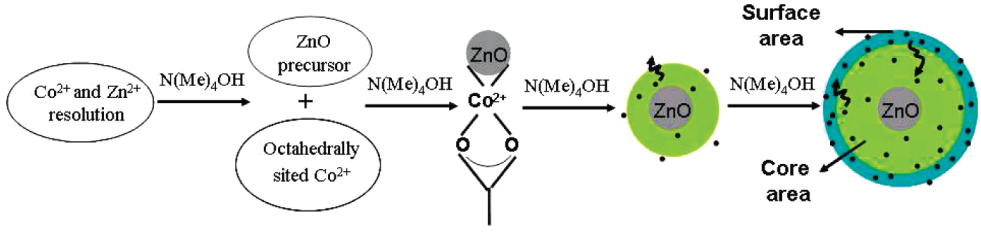

FIGURE 3. Sketches of detailed self-purification process.

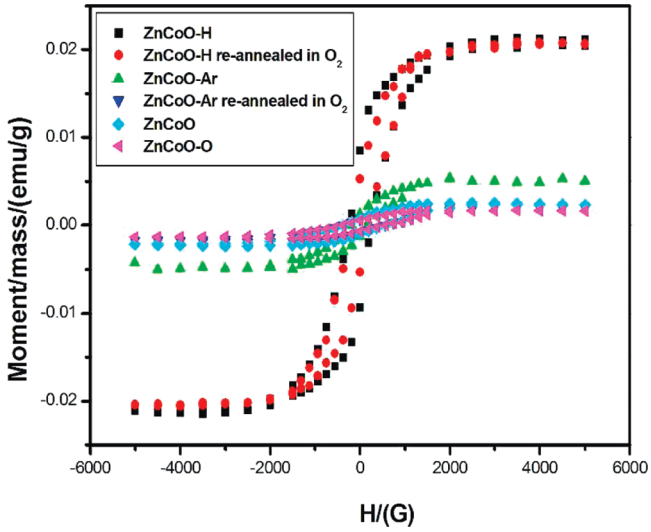

FIGURE 4. $M-H$ curves detected at 300 K for as-prepared and postannealed $Zn_{0.95}Co_{0.05}O$ nanocrystals.

nanocrystals decreases a little, but it increases obviously after Ar or H_2 annealing. The largest ferromagnetism is observed in ZnCoO-H, that value of which is 11 times that of ZnCoO. It is well-known that V_os are common defects in *n*-type ZnO and it can mediate the spin−spin ferromagnetic coupling between transition metal ions (25, 26). To verify whether the ferromagnetism enhancement is related to the V_o's concentration variation after annealing, we have deliberately reannealed ZnCoO-Ar and ZnCoO-H in oxygen. It is found that the magnetization of the ZnCoO-Ar recovers to the value of ZnCoO, whereas the magnetization hardly changes in ZnCoO-H. This fact indicates that the origin of ferromagnetism enhancement of ZnCoO-H is different from that of ZnCoO-Ar. For ZnCoO-Ar, the magnetization increase could be attributed to the increase of V_o's concentration after annealing in Ar. After reannealing in O_2, the V_o's concentration recovers to the value of ZnCoO, as does the magnetism. However, the ferromagnetism enhancement in ZnCoO-H could not be explained by the variation in V_o's concentration alone, as the ferromagnetism is unchanged after reannealing in oxygen. H_2 postannealing must have introduced other structure changes into the $Zn_{0.95}Co_{0.05}O$ nanocrystals. As reannealing in oxygen does not obviously change the ferromagnetism, the formation of Co metal clusters due to the reduction effect H_2 could be ruled out. If Co metal clusters appear in the nanocrystals, they can be oxidized by reannealing in oxygen and the magnetism should decline.

3.4. XPS Study. Figure 5 shows the XPS spectra of ZnCoO, ZnCoO-O, ZnCoO-Ar, ZnCoO-H, and Co metal nanoparticles. The Co $2p_{3/2}$ peak at 780−781 eV is distinct from Co metal peak at 778.8 eV. The separation between Co $2p_{3/2}$ and Co $2p_{1/2}$ is about 15.8 eV, which is larger than that of Co metal (15.06 eV). The two shakeup satellite peaks on the higher binding energies are the typical characteristics of

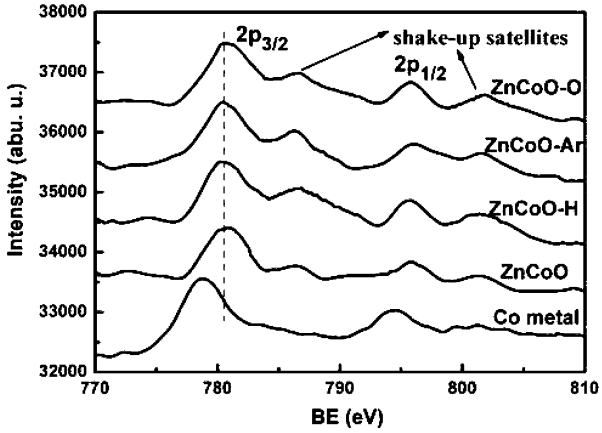

FIGURE 5. XPS spectra of ZnCoO-O, ZnCoO-Ar, ZnCoO-H, ZnCoO, and commercial Co metal nanoparticles.

high-spin Co^{2+} due to the charge-transfer band structure of the cobalt monoxides, which indicates that the Co ions are primarily in high-spin electronic state ($3d^7$, $S = 3/2$) (27, 28). These results reveal that Co ions mainly substitute Zn ions in $Zn_{0.95}Co_{0.05}O$, other than existing in the interstitial sites. The interstitial Co atoms have been proved to take the low-spin states (29, 30). It is noted that the Co $2p_{3/2}$ peak of ZnCoO-O appears at higher energy (at 780.9 eV) than those of ZnCoO-Ar (at 780.6 eV) and ZnCoO-H (at 780.5 eV). This is clear evidence of the increase in the V_o's concentration. During the annealing process in Ar and H_2 where the oxygen partial pressure is zero, oxygen atoms near the surface will gain sufficient energy to diffuse out of the nanocrystals and thus leave V_os in the crystal lattice. The relatively high annealing temperature provides sufficient energy for the V_os to diffuse in the nanocrystals. As a result, the average number of oxygen ions binding with Co ions decreases and the Co−O bonds stretch for the lattice relaxation. Therefore, the binding energy of the Co 2p electrons decreases. Similar phenomena have been observed in $Sn_{1-x}Co_xO_2$ system (31).

3.5. FT-Raman Study. Figure 6 shows the Raman spectra of $Zn_{0.95}Co_{0.05}O$ nanocrystals before and after post-annealing. The peaks at 97, 201, 333, 437, 483, 536, 578, 666, 985, and 1146 cm^{-1} are referred to typical Raman vibration modes of E_{2L}, $2E_{2L}$, $E_{2H}-E_{2L}$, E_{2H}, 2LA, $2B_{1L}$, A_{1L} or E_{1L} or LO, TA + LO, 2TO, and $2A_{1L}$, or $2E_{1L}$ for Wurtzite ZnO, respectively (12, 32, 33). Obvious changes are observed at peak a around 670 cm^{-1} (TA + LO mode). In the ZnCoO-O spectrum, peak a rises up and broadens remarkably to the high-frequency side. As shown in the inset of Figure 6a, the peak a of ZnCoO-O can be decomposed into two peaks at 666 cm^{-1} (TA + LO mode of wurtzite structured ZnO) and 695 cm^{-1} (A_{1g} mode of Co_3O_4 Spinel, Co in octahedral field) by careful Gauss fitting (11, 34, 35). This clearly shows that second-phase spinel Co_3O_4 forms in ZnCoO-O. Because Co_3O_4 is antiferromagnetic and the formation of the Co_3O_4 clusters obstructs the exchange interaction between the Co^{2+} ions in tetrahedral field place, the ferromagnetism of ZnCoO-O declines. The integration intensity of the 695 cm^{-1} peak corresponds to the concentration of Co ions occupied the octahedral interstitial sites. Its variation for different annealing atmospheres is sketched in Figure 6b. It is found

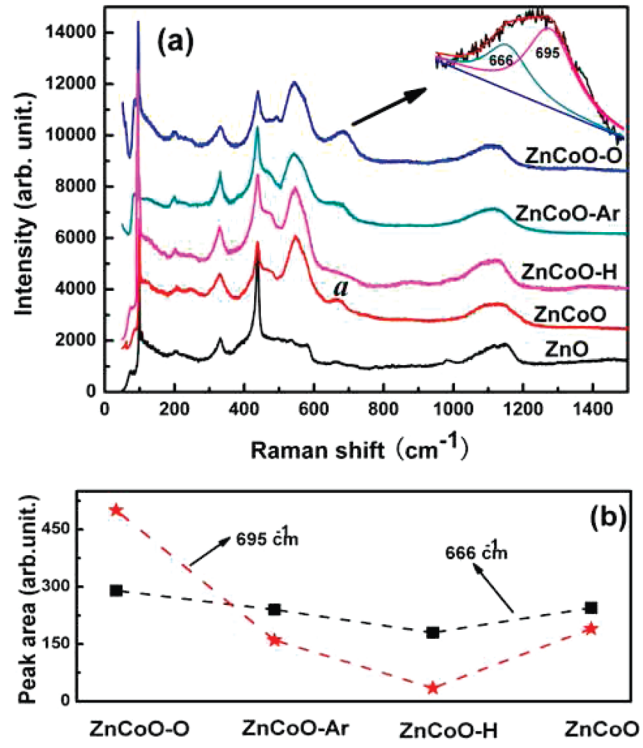

FIGURE 6. (a) Raman spectra of pure ZnO, as-prepared, and post-annealed $Zn_{0.95}Co_{0.05}O$ nanocrystals. The inset shows the Gauss fitting of the peak *a* of ZnCoO-O. (b) Variation in peak areas of the peak 666 and 695 cm^{-1} obtained by Gauss fitting of peak *a*.

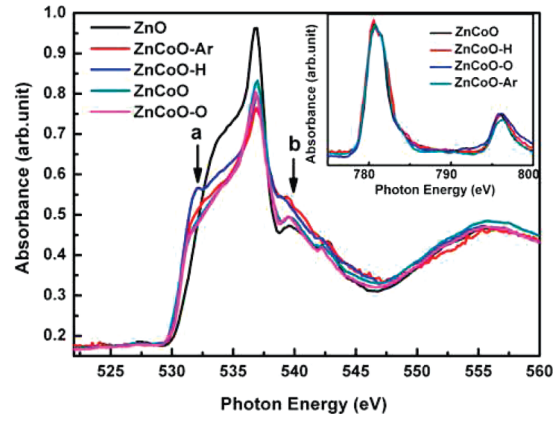

FIGURE 7. XNEAS at the O K-edge and the Co $L_{2,3}$-edge (inset) collected at 300 K for pure ZnO, as-prepared, and postannealed $Zn_{0.95}Co_{0.05}O$ nanocrystals.

that ZnCoO has a low intensity at 695 cm^{-1}, which implies that there are some Co ions occupying the octahedral interstitial sites when Co concentration approaches the solubility. Compared with ZnCoO, the 695 cm^{-1} peak intensity of ZnCoO-H sample decreases to about zero, but that of the ZnCoO-O sample increases greatly. This suggests that Co ions in the octahedral field decreased in ZnCoO-H, but increased in ZnCoO-O. The increase in octahedrally sited Co ions in ZnCoO-O results from the appearance of spinel Co_3O_4.

3.6. XNEAS Spectra. Figure 7 shows the XNEAS spectra of all the $Zn_{0.95}Co_{0.05}O$ samples. The XNEAS spectrum of pure ZnO single crystal is also given for comparison. Co $L_{2,3}$-edge spectra (the inset of Figure 7) indicate that most

of the Co atoms are doped into ZnO lattice and forms solid-solution $Zn_{1-x}Co_xO$, which further rules out the presence of Co metal clusters (36, 37). The hybridization of O 2p orbital and the orbital of Zn and Co is shown in the O K-edge XNEAS, which can be divided into 3 stages. The region between 530−538 eV is attributed to O 2p-Zn 4*s* hybridized states and the sharp peak at around 537 eV is due to the transition of O 1s electrons to more localized O $2p_z$ and $2p_{x+y}$ states; the region between 538 and 550 eV arises from O 2p states hybridized with Zn 4p states; and the region after 550 eV is assigned to O 2p states hybridized with Zn 4d states. The broadening of the spectral feature at 537−540 eV (feature b) results from the increase of oxygen vacancies (37, 38). It is found that feature b of the ZnCoO-Ar and ZnCoO-H samples have similar intensity, but it is obviously higher than that of ZnCoO. This further proves the increase of V_o's concentration by Ar or H_2 postannealing, which is coincident with the XPS results. The notable difference lies at feature a at 531−532 eV, where ZnCoO-H has a much higher intensity than ZnCoO-Ar and other samples. This near-edge feature was recently assigned to the presence of V_os or the hybrid of Co 3d with O 2p state related to defect structures (37−39). Because both the V_o's intensities of ZnCoO-H and ZnCoO-Ar increases just as denoted at feature b, the intensity difference of feature a could hardly be attributable the increasing of V_os. It could originate only from the change of the Co 3d and O 2p hybrid state resulting from H_2 postannealing. Hydrogen is well-known as an unintentional dopant of a significant concentration in the ZnO, and is considered as the major shallow donor in the natural *n*-type character of ZnO (40, 41). During H_2 postannealing, a great number of H atoms are introduced into $Zn_{0.95}Co_{0.05}O$ system. These H atoms mainly occupy the interstitial positions of the lattice. Theoretical simulation indicates that H_is can locate at the center of Co−O bonds or form Co−H−Co bridge bond structures with two adjacent substitutional Co ions, but the latter is energy-preferential (42, 43). H_is in $Zn_{1-x}Co_xO$ can interact with Co impurity ions by the capture of its shallow donor electron through the Co-3d-t_{2g} orbital at the gap top (44). This means the H_i related defect structures have great effects on the 3d−2p coupling in $Zn_{1-x}Co_xO$. Thus, the increase of the feature a intensity in ZnCoO-H should be related to the increase in H_i and related defects, such as Co−H−Co bridge bond structures.

3.7. Magnetic Coupling Mechanism. Coey et al. proposed a bound magnetic polaron (BMP) model to explain the magnetic coupling in $Zn_{1-x}Co_xO$ DMSs, which indicated that shallow donor electrons bounded to *p*-type defects formed BMPs or created a spin-split impurity band (45, 46). The BMPs or spin-split impurity band could mediate ferromagnetic interaction between the transition metal ions. Our results indicate the V_o's concentration increase in ZnCoO-Ar, and ZnCoO-H samples. There are not other *p*-type dopants in our experiment. V_o is typical positively charged defects, and it can play same role as the *p*-type defects. We speculate that the electron may be bound to V_os formed bound magnetic polarons (BMPs) and created a spin split impurity band. In our opinion, two kinds of mechanisms may be coexistent in our samples. One reason is that V_os promote the magnetism because they strengthen the Co−Co magnetic interaction when Co ions at nearest position. The other one results from increase of BMPs. However, the significant ferromagnetism of enhancement of ZnCoO-H could hardly be explained only by BMP model. The H_is may play the most important role in mediating the magnetic coupling in ZnCoO-H. Theoretical simulation indicated that H_i could mediate a strong short-range ferromagnetic spin−spin interaction between neighboring Co impurities by forming a Co−H−Co bridge bond structure (40, 41). This Co−H−Co bridge structure may be responsible for the great ferromagnetism enhancement of ZnCoO-H. Figure 8 shows the sketches for crystal lattice and the energy level of the ZnCoO and ZnCoO-H samples (40, 47). Because the Co distribution of $Zn_{0.95}Co_{0.05}O$ nanocrystals are of surface-preferential, the Co concentration at the surface area is much higher. Thus there are some Co ions located at interstitial sites, just as proved by the Raman results. As shown in Figure 8a, the interstitially (octahedrally) located Co ions are in low-spin state and their spins are antiparallel to that of the adjacent substitutional (tetrahedral) Co ions owing to the direct-exchange mechanism. Therefore, the ferromagnetism of ZnCoO is relatively weak. When the nanocrystals are annealed under H_2, a lot of H_is are incorporated into the sample, thus Co−H−Co bridge structures form by consuming the interstitial Co ions for lowering the system energy (42). As shown in Figure 8b, in this case, the spins of the two neighboring substitutional (tetrahedral) Co ions become parallel via the H_i mediator. This Co−H−Co bridge structure leads to the great enhancement of the ferromagnetism in ZnCoO-H. Because the Co−H−Co structures are energy-preferential, they are so stable they could not be destroyed by being annealed at 673 K in oxygen. This might be the reason why the magnetization of ZnCoO-H remains unchanged after reannealing in oxygen at 673 K. To analyze the effects of H_i, the magnetization of samples annealed in different volume ratio have been studied. From Figure 9, it is found that the ferromagnetism enhances with the increasing of H_2 volume ration. This further evidence indicates that H_2 postannealing must have introduced structure changes into the $Zn_{0.95}Co_{0.05}O$ nanocrystals. The formation of Co−H−Co bridge structure needs certain H_2 concentration.

The experimental results also suggest that the inhomogeneous distribution of Co is a critical factor for modulating the state of the Co ions by postannealing. Just because of surface-preferential Co distribution, the Co concentration at the surface area is large. Thus V_o can mediate the magnetic exchange between Co ions more effective, second-phase Co_3O_4 and Co−H−Co bridge structures can form easily during O_2 or H_2 annealing for the short average distance between Co ions. The inhomogeneous distribution of TM ions is a general state in ZDMSs and it has important effects on the magnetism properties (9, 12, 13, 48). This inhomogeneous distribution of TM may provides a way for understanding the current controversial experimental results that

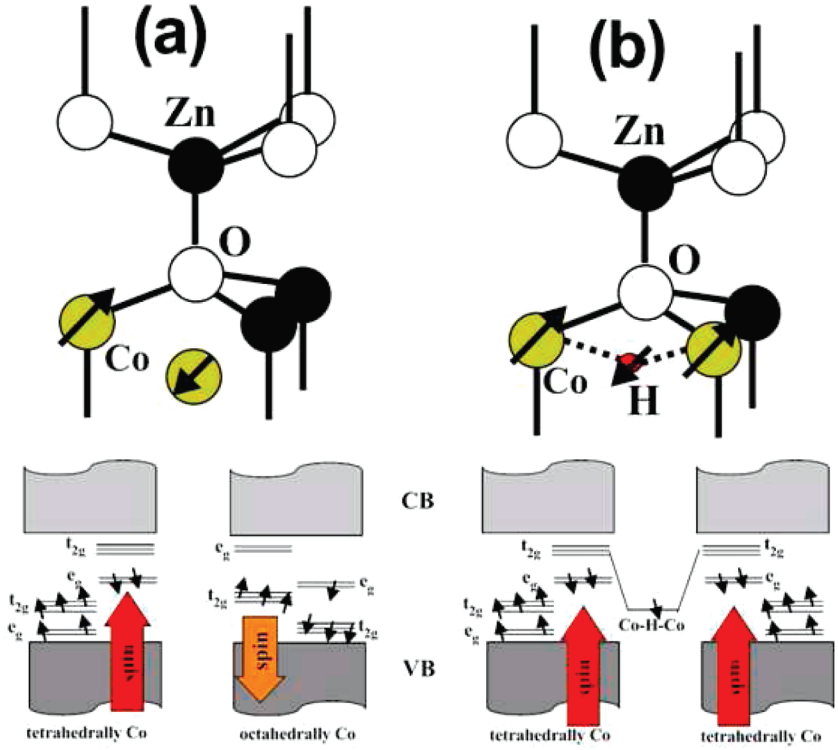

FIGURE 8. Crystal lattice and energy level sketches of (a) ZnCoO and (b) ZnCoO-H.

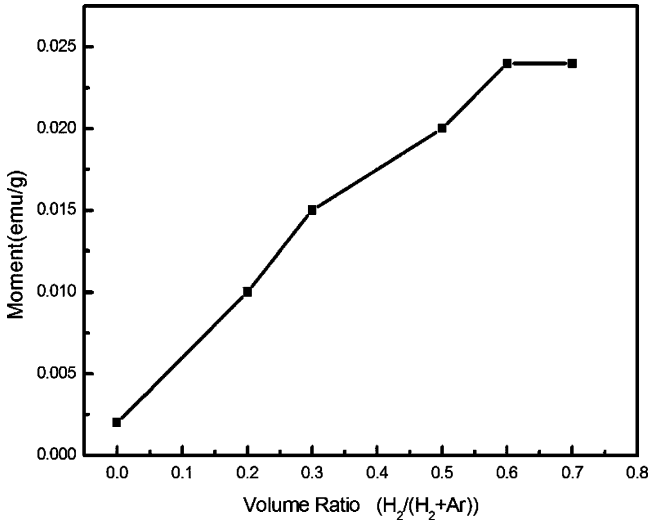

FIGURE 9. Magnetizations of ZnCoO-H samples annealed with different H_2 volume ratios.

many highly crystallized ZDMSs films show no or very weak ferromagnetism, whereas the less-crystallized ZDMSs, especially nanocrystals, often show relatively strong room-temperature ferromagnetism. The inhomogeneous TM distribution in ZDMSs can also explain why the magnetic properties can be well-modulated by various surface treatments (15, 49).

4. CONCLUSIONS

In summary, STEM image presents solid evidence that Co element distribution in ZnO nanocrystals is of surface-preferential. Our results indicate that this inhomogeneous Co distribution is helpful for manipulating the states of the Co ions and the ferromagnetic coupling in $Zn_{1-x}Co_xO$ by post-treatment. The variations of ferromagnetism in ZnCoO-O and ZnCoO-Ar are owing to the formation of second-phase Co_3O_4 and the increase of V_os, respectively. The great enhancement of the ferromagnetism in ZnCoO-H is attributed to the formation of Co−H−Co stable structures. Just because of surface-preferential Co distribution, the Co concentration at the surface area is large. Thus V_o can mediate the magnetic exchange between Co ions more effective, second-phase Co_3O_4 and Co−H−Co bridge structures can form easily during O_2 or H_2 annealing for the short average distance between Co ions. This inhomogeneous distribution of TM should be seriously taken into account in future DMS studies.

Acknowledgment. This work was financially supported by National Nature Science Foundation of China (Grant 60776067) and Spaceflight Basic Research Fund. The XNEAS measurements were performed on synchrotron radiation at Beijing Synchrotron Radiation Facility in Institute of High Energy Physics, Chinese Academy of Science.

REFERENCES AND NOTES

(1) Prinz, G. A. *Science* **1998**, *282*, 1660.
(2) Dietl, T.; Ohno, H.; Matsukura, F.; Cibert, J.; Ferrand, D. *Science* **2000**, *287*, 1019.
(3) Sato, K.; Katayama-Yoshida, H. *Jpn. J. Appl. Phys.* **2000**, *40*, L334.
(4) Ueda, K.; Tabata, H.; Kawai, T. *Appl. Phys. Lett.* **2001**, *79*, 988.
(5) Rode, K.; Anane, A.; Mattana, R. *J. Appl. Phys.* **2003**, *93*, 7676.
(6) Pemmaraju, C. D.; Hanafin, R.; Archer, T.; Braun, H. B.; Sanvito, S. *Phys. Rev. B* **2008**, *78*, 054428.
(7) Ando, K.; Saito, H.; Zayets, V.; Debnath, M. C. *J. Phys: Condens. Matter.* **2004**, *16*, S5541.
(8) Chambers, S. A.; Droubay, T. C.; Wang, C. M.; Rosso, K. M.; Heald, S. M.; Schwartz, D. A.; Kittilstved, K. R.; Gamelin, D. R. *Mater. Today* **2006**, *9*, 28.
(9) Dietl, T.; Andrearczyk, T.; Lipińska, A.; Kiecana, M.; Tay, M.; Wu, Y. *Phys. Rev. B* **2007**, *76*, 155312.

(10) Fukuma, Y.; Asada, H.; Yamamoto, J.; Odawara, F.; Koyanagi, T. *Appl. Phys. Lett.* **2001**, *93*, 142510.
(11) Wang, X. F.; Xu, J. B.; Yu, X. J.; Xue, K.; Yu, J. G.; Zhao, X. J. *Appl. Phys. Lett.* **2007**, *91*, 031908.
(12) Iusan, D.; Kabir, M.; Gråsäs, O.; Eriksson, O.; Sanya, B. *Phys. Rev. B* **2009**, *79*, 125202.
(13) Zhang, Y. B.; Assadi, M. H. N.; Li, S. *J. Phys: Condens. Matter.* **2009**, *21*, 175802.
(14) Pan, F.; Song, C.; Liu, X. J.; Yang, Y. C.; Zeng, F. *Mater. Sci. Eng., R* **2008**, *62*, 1.
(15) Hong, N. H.; Sakai, J.; Huong, N. T.; Poirot, N.; Ruyter, A. *Phys. Rev. B* **2005**, *72*, 045336.
(16) Risbud, A. S.; Spaldin, N. A.; Chen, Z. Q.; Stemmer, S.; Seshadri, R. *Phys. Rev. B* **2003**, *68*, 205202.
(17) Samanta, K.; Bhattacharya, P.; Katiyar, R. S.; Iwamoto, W.; Pagliuso, P. G.; Rettori, C. *Phys. Rev. B* **2006**, *73*, 245213.
(18) Wang, X. F.; Xu, J. B.; Zhang, B.; Yu, H. G.; Wang, J.; Zhang, X. X.; Yu, J. G.; Li, Q. *Adv. Mater.* **2006**, *18*, 2476.
(19) Li, J. J.; Hao, W. C.; Xu, H. Z.; Wang, T. M. *J. Appl. Phys.* **2009**, *105*, 053907.
(20) Ma, J.; Hao, W. C.; Luo, R.; Xu, H. Z. *Mater. Lett.* **2008**, *62*, 403.
(21) Schwartz, D. A.; Norberg, N. S.; Nguyen, Q. P.; Parker, J. M.; Gamelin, D. R. *J. Am. Chem. Soc.* **2003**, *125*, 1320.
(22) Mikulec, F. V.; Kuno, M.; Bennati, M.; Hall, D. A.; Griffin, R. G.; Bawendi, M. G. *J. Am. Chem. Soc.* **2000**, *122*, 2532.
(23) Dalpian, G. M.; Chelikowsky, J. R. *Phys. Rev. Lett.* **2006**, *96*, 206802.
(24) Norris, D. J.; Efros, A. L.; Erwin, S. C. *Science* **2008**, *319*, 1776.
(25) Patterson, C. H. *Phys. Rev. B* **2006**, *74*, 144432.
(26) Liu, X. C.; Shi, E. W.; Chen, Z. Z. *J. Phys: Condens. Matter.* **2008**, *20*, 025208.
(27) Garson, G. A.; Nassir, M. H.; Langell, M. *J. Vac. Sci. Technol., A* **1996**, *14*, 1637.
(28) Towle, S. N.; Bargar, J. R.; Brown, G. E., Jr.; Parks, G. A. *J. Colloid Interface Sci.* **1997**, *187*, 62.
(29) Quilty, J. W.; Shibata, A.; Son, J. Y.; Takubo, K.; Mizokawa, T.; Toyosaki, H.; Fukumura, T.; Kawasaki, M. *Phys. Rev. Lett.* **2006**, *96*, 027202.
(30) Geng, W. T.; Kim, K. S. *Phys. Rev. B* **2003**, *68*, 125203.
(31) Liu, X. F.; Sun, Y.; Yu, R. H. *J. Appl. Phys.* **2007**, *101*, 123907.
(32) Calleja, J. M.; Cardona, M. *Phys. Rev. B* **1977**, *16*, 3753.
(33) Cuscó, R.; Alarcón-Lladó, E.; Ibáñez, J.; Artús, L.; Jiménez, J.; Wang, B.; Callahan, M. J. *Phys. Rev. B* **2007**, *75*, 165202.
(34) Windisch, C. F.; Exarhos, G. J.; Owings, R. R. *J. Appl. Phys.* **2004**, *95*, 5435.
(35) Hadjiev, V. G.; Iliev, M. N.; Vergilov, I. V. *J. Phys. C: Solid State Phys.* **1988**, *21*, L199.
(36) Wi, S. C.; Kang, J.-S.; Kim, J. H.; Cho, S.-B.; Kim, B. J.; Yoon, S.; Suh, B. J.; Han, S. W.; Kim, K. H.; Kim, K. J.; Kim, B. S.; Song, H. J.; Shin, H. J.; Shim, J. H.; Min, B. I. *Appl. Phys. Lett.* **2004**, *84*, 4233.
(37) Krishnamurthy, S.; McGuinness, C.; Dorneles, L. S.; Venkatesan, M.; Coey, J. M. D.; Lunney, J. G.; Patterson, C. H.; Smith, K. E.; Learmonth, T.; Glans, P. -A.; Schmitt, T.; Guo, J.-H. *J. Appl. Phys.* **2006**, *99*, 08M111.
(38) Singh, A. P.; Kumar, R.; Thakur, P.; Brookes, N. B.; Chae, K. H.; Choi, W. K. *J. Phys: Condens. Matter.* **2009**, *18*, 185005.
(39) Song, C.; Pan, S. N.; Liu, X. J.; Li, X. W.; Zeng, F.; Yan, W. S.; He, B.; Pan, F. *J. Phys: Condens. Matter.* **2007**, *19*, 176229.
(40) Cox, S. F. J.; Davis, E. A.; Cottrell, S. P.; King, P. J. C.; Lord, J. S.; Gil, J. M. *Phys. Rev. Lett.* **2001**, *86*, 2601.
(41) Strzhermechny, Y. M.; Mosbacker, H. L.; Look, D. C.; Reynolds, D. C.; Litton, C. W.; Garces, N. Y. *Appl. Phys. Lett.* **2004**, *84*, 2545.
(42) Park, C. H.; Chadi, D. J. *Phys. Rev. Lett.* **2005**, *94*, 127204.
(43) Wardle, M. G.; Goss, J. P.; Briddon, P. R. *Phys. Rev. B* **2005**, *72*, 155108.
(44) Sato, K.; Katayama-Yoshida, H. *Jpn. J. Appl. Phys.* **2000**, *39*, L555.
(45) Coey, J. M. D.; Douvalis, A.; Fitzgerald, C. B.; Venkatesan, M. *Appl. Phys. Lett.* **2004**, *84*, 1332.
(46) Coey, J. M. D.; Venkatesan, M.; Fitzgerald, C. B. *Nat. Mater.* **2005**, *4*, 173.
(47) Sato, K.; Katayama-Yoshida, H. *Semicond. Sci. Technol.* **2002**, *17*, 367.
(48) Straumal, B.; Baretzky, B.; Mazilkin, A.; Protasova, S.; Myatiev, A.; Straumal, P. *J. Eur. Ceram. Soc.* **2009**, *29*, 1963.
(49) Kittilstved, K. R.; Norberg, N. S.; Gamelin, D. R. *Phys. Rev. Lett.* **2005**, *94*, 147209.

AM100303N